KEK-preprint-93-215 TUAT-HEP 94-1 DPNU-94-11 TIT-HPE-94-01 NWU-HEP 94-01 OCU-HEP 94-1 PU-94-681 KOBE-HEP 94-03

Measurement of the $D^{*\pm}$ Cross Section using a Soft-Pion Analysis in Two-Photon Processes *

TOPAZ Collaboration

R.Enomoto^{a,†}, K.Abe^b, T.Abe^c, I.Adachi^a, M.Aoki^c, M.Aoki^d, S.Awa^e R.Belusevic^a, K.Emi^b, H.Fujii^a, K.Fujii^a, T.Fujii^f, J.Fujimoto^a, K.Fujita^g, N.Fujiwara^e, H.Hayashii^e, B.Howell^h, N.Iida^a, H.Ikeda^a, R.Itoh^a, H.Iwasaki^a, M.Iwasaki^e, R.Kajikawa^c, K.Kaneyuki^d, S.Katoⁱ, S.Kawabata^a, H.Kichimi^a, M.Kobayashi^a, D.Koltick^h, I.Levine^h, S.Minami^d, K.Miyabayashi^c, A.Miyamoto^a, K.Muramatsu^e, K.Nagai^j, T.Nagira^e, E.Nakano^c, K.Nakabayashi^c, O.Nitoh^b, S.Noguchi^e, F.Ochiai^k, Y.Ohnishi^c, H.Okunoⁱ, T.Okusawa^g, K.Shimozawa^c, T.Shinohara^b, A.Sugiyama^c, N.Sugiyama^d, S.Suzuki^c, K.Takahashi^b, T.Takahashi^g, M.Takemoto^e, T.Tanimori^d, T.Tauchi^a, F.Teramae^c, Y.Teramoto^g, N.Toomi^e, T.Toyama^c, T.Tsukamoto^a, S.Uno^a, T.Watanabe^d, Y.Watanabe^d, A.Yamaguchi^e, A.Yamamoto^a, and M.Yamauchi^a

```
<sup>a</sup> National Laboratory for High Energy Physics, KEK, Ibaraki-ken 305, Japan
```

Abstract

The differential cross section of $d\sigma(e^+e^- \to e^+e^-D^{*\pm}X)/dP_T$ was measured using a soft-pion analysis of $D^{*\pm} \to \pi_s^{\pm}D^0(\overline{D^0})$ at TRISTAN. The average \sqrt{s} was 58.1 GeV and the integrated luminosity used in this analysis was 198 pb⁻¹, respectively.

1 Introduction

Multi-hadron production in two-photon processes is qualitatively described using the vector-meson dominance model (VDM), the quark-parton model (direct process) [1], and resolved photon processes [2, 3, 4, 5, 6, 7]. In order to understand them quantitatively, charm production is a good proof, because

^bDept. of Applied Physics, Tokyo Univ. of Agriculture and Technology, Tokyo 184, Japan

^cDepartment of Physics, Nagoya University, Nagoya 464, Japan

^dDepartment of Physics, Tokyo Institute of Technology, Tokyo 152, Japan

^eDepartment of Physics, Nara Women's University, Nara 630, Japan

^f Department of Physics, University of Tokyo, Tokyo 113, Japan

^gDepartment of Physics, Osaka City University, Osaka 558, Japan

^hDepartment of Physics, Purdue University, West Lafayette, IN 47907, USA

ⁱInstitute for Nuclear Study, University of Tokyo, Tokyo 188, Japan

^j The Graduate School of Science and Technology, Kobe University, Kobe 657, Japan

^k Faculty of Liberal Arts, Tezukayama Gakuin University, Nara 631, Japan

^{*}published in Phys. Lett. **B 328** (1994) 535.

[†]Email address: enomoto@kekvax.kek.jp

the theoretical calculations have been completed to higher order (order α_s) [8, 9]. In addition, cut-off parameters, such as P_T^{min} , are not necessary in the theoretical calculation [10, 11] and the background from the VDM is considered to be very small. Studies of charm-meson production should provide useful information concerning the gluon density in a photon, the current charm quark mass, and the intrinsic P_T distribution of the partons in resolved photons. The statistics of the previous experiments were too poor to determine these parameters [12, 13, 14].

In a previous measurement by TOPAZ using the decay mode $D^{*+} \to \pi_s^+ D^0(D^0 \to K^-\pi^+ X)$ as well as its charge-conjugation mode (CC) [15], an excess in charm production compared with the theoretical expectation was shown [9]. Super-symmetric particle production (\tilde{t}) is one possible interpretation of this experimental excess [16, 17, 18, 19, 20]. However, the accuracy of the experiment was not good enough to justify this assumption. For the above-mentioned reasons, more precise measurements of charm production in two-photon processes have been awaited.

2 Analysis

2.1 Soft-pion analysis of $D^{*+} \to \pi_s^+ D^0$

The decay $D^{*\pm} \to \pi_s^\pm D^0(\bar{D}^0)$ is characterized by its small Q value. The maximum transverse momentum of π_s^\pm (soft-pion or π_s from hereafter) with respect to the D^0 (from hereafter, the descriptions of the charge states include their charge conjugations) flight direction is only 40 MeV. Its direction can be approximated by the jet-axis obtained by an invariant mass algorithm [21]. Therefore, from the distribution of the transverse momenta of soft-pions with respect to the jet-axes $(P_{T,jet}^2)$, the production cross section of $D^{*\pm}$ can be precisely measured. The acceptance of this method was proven to be one order higher than that of the exclusive reconstruction of $D^{*\pm}$ decay [21]. We thus tried this method for two-photon events, and obtained the differential cross section of $D^{*\pm}$ as a function of P_T , the transverse momentum with respect to the beam axis. Higher statistics and lower systematic error measurements were expected using this analysis.

2.2 Data sample

The data were obtained by the TOPAZ detector at the TRISTAN e^+e^- collider of KEK. The details concerning the TOPAZ detector can be found elsewhere [22]. The integrated luminosity of the event sample used in the analysis was 198 pb⁻¹. The average \sqrt{s} was 58.1 GeV. The trigger conditions were as follows: more than two tracks with $P_T > 0.3 \sim 0.7$ GeV and an opening angle $> 45 \sim 90$ degrees (depending on the beam condition); the neutral energy deposit in the barrel calorimeter be greater than $2 \sim 4$ GeV; or that in the endcap calorimeter be greater than 10 GeV.

The event selection criteria for the two-photon process were tighter than in the exclusive $D^{*\pm}$ analysis [15], because this signal suffered from the background of the VDM as well as single-photon exchange hadronic events. The selections were as follows: the number of charged tracks be ≥ 4 ; the total visible energy in the central part of the detector be between 5 and 25 GeV; the vector sum of the transverse momenta of the particles with respect to the beam axis be less than 7.5 GeV; the absolute value of the sum of charges be ≤ 3 ; the absolute value of the cosine of the thrust axis in the laboratory frame be less than 0.9, where neutral clusters detected by the endcap calorimeters were included; and no large energy clusters in the barrel calorimeter ($E > 0.25E_{beam}$). In addition, we divided each event into two jets with respect to the plane perpendicular to the thrust axis at the laboratory frame; the cosine of the angle between two jets was required to be greater than -0.9. These cuts were determined using a Monte-Carlo simulation of the direct process events so as to maximize the charm event acceptance and its purity. A total of 14128 events were selected.

2.3 Particle selection

The charged track selections were as follows: the closest approach to the event vertex be consistent within the measurement error; the number of degrees of freedom (DOF) in the track-fitting be ≥ 3 ; and P_T be ≥ 0.1 GeV. The γ selections were: the cluster be detected by a barrel calorimeter; the energy be ≥ 0.2 GeV; and the cluster position be separated from any charged-track extrapolations by more than 10 cm at the surface of the barrel calorimeter.

2.4 Jet-axis determination

The jet-axis was obtained by using an invariant mass algorithm [21], in which particles were merged together in an iterative way if their invariant mass was less than 2 GeV. In this algorithm, a soft-pion candidate, whose $P_{T,jet}^2$ must be calculated, was removed from the sample particles, i.e., the jet-axis was recalculated each time when a particle was selected to be the soft-pion candidate. Then, those jet candidates having invariant masses greater than 0.3 GeV and transverse momenta with respect to the beam-axis of greater than 1 GeV were selected. The former cut were to remove jets made of single track. The fake tracks by the patter recognition (duplicating tracks using the same space-points) were removed from the charged track sample. By the above algorithm, two or three jets were usually reconstructed (85% of the events).

Those cut values were determined using a Monte-Carlo simulation while assuming a direct process. The best angular resolution of the soft-pions with respect to the jet-axes was obtained using the above set of cut values. Even when the jet-mass was as low as 0.3 GeV, the D^0 direction was calculated with the acceptable resolution which was proven by a Monte-Carlo simulation. The estimated angular resolution of the soft-pions was approximated by $e^{3.7-4.3P_T}$ degrees (P_T in GeV). The transverse momentum resolutions with respect to the jet-axis were 70 ± 10 MeV in the P_T region between 0.1 and 0.6 GeV, a slowly increasing function of the soft-pion's P_T .

The transverse momentum of the soft-pion was calculated with respect to the closest jet candidate $(P_{T,iet}^2)$.

The effects by the pair conversion electron and Dalitz pairs were estimated using a Monte-Carlo simulation. They were proven to be absorbed in the background function in the fitting procedure which is described in Section 2.6.2.

2.5 $P_{T,jet}^2$ distribution of soft-pions

The P_T range of the soft-pion candidates was set to $0.1 < P_T < 0.6$ GeV in order to cover the predicted region by the direct process. The $P_{T,jet}^2$ distribution for the above-mentioned P_T range is plotted in Figure 1 (a). There is a clear peak at around the zero $P_{T,jet}^2$ region.

In order to derive the differential cross section with respect to P_T , we selected the following P_T ranges: (b) $0.1 < P_T < 0.2$, (c) $0.2 < P_T < 0.3$, (d) $0.3 < P_T < 0.4$, and (e) $0.4 < P_T < 0.6$ GeV. The corresponding distributions are shown in Figures 1 (b), (c), (d), and (e), respectively. The binning was selected so as to give similar peak entries. The resolution of the P_T 's of the soft-pions are smaller than these binnings.

2.6 Background estimation

2.6.1 Monte-Carlo simulations

In the soft-pion analysis, background emulation using the experimental data is difficult, in contrast to the case in a full-reconstruction analysis, where wrong sign combinations can be used to emulate the background [15]. We therefore used a Monte-Carlo method. The $\gamma\gamma$ generation was based on an equivalent photon approximation. For the parton generations, we used lowest-order formulas (Born

Figure 1: Distributions of $P_{T,jet}^2$ of soft-pion candidates: (a) for $0.1 < P_T < 0.6$ GeV, (b) $0.1 < P_T < 0.2$, (c) $0.2 < P_T < 0.3$, (d) $0.3 < P_T < 0.4$, and (e) $0.4 < P_T < 0.6$. The dashed lines are the result of a Monte-Carlo simulation of the background, where the normalizations were carried out using the entries of $P_{T,jet}^2 > 0.02$ GeV. The hatched histograms are contributions from $e^+e^- \to (\gamma) \to D^{*\pm}X$. The solid curves are the best-fitted functions which are described in the text. The higher lines are signals and backgrounds, and the lower are backgrounds.

approximation). In the resolved photon processes, LAC1 [6] parametrization was used for the parton density in the photon. For light-quark event generation, a P_T^{min} of 2.5 GeV was used, which was the best-fitted value using the general event shapes of a $\gamma\gamma \to$ (multi-hadrons) obtained by the TOPAZ detector [11]. In addition, the VDM Monte-Carlo events and $e^+e^- \to \gamma \to q\bar{q}$ events by the LUND 6.3 (parton shower option) program were added. In LUND 6.3, the branching ratios of D^0 were adjusted to the PDG values [23]. Hadronization of partons generated by the $\gamma\gamma$ events was carried out using LUND 6.3 string fragmentation without a parton shower option [24]. A more detailed description together with a detector simulation can be found in Reference [11].

The branching ratio of $D^{*+} \to \pi_s^+ D^0$ was assumed to be 68.1%, which was obtained by CLEO [25]. The V/(V+P) ratio was set to 0.75 and a u:d:s:qq ratio of 1:1:0.3:0.1 was used.

The results of this Monte-Carlo simulation are shown in Figures 1 (a) - (e) by the dashed lines. The events with $D^{*\pm} \to \pi^{\pm} D^0(\overline{D^0})$ were removed from these. They fit with the experimental data in the higher P_T regions. In the lower P_T region, however, since the agreement of the normalization scale was poor, the lines in Figure 1 were normalized using the entries of $P_{T,jet}^2 > 0.02$ GeV. However, the background shape (i.e., in the higher $P_{T,jet}^2$ region) agreed well. The contributions from $e^+e^- \to \gamma \to D^{*\pm}X$ are shown in Figures 1 (a) - (e) by hatched histograms, and are considered to be negligible.

2.6.2 Fit of the $P_{T,jet}^2$ spectra

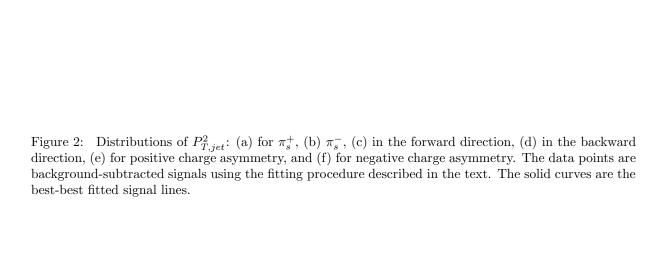
There is a difference between the experimental and Monte-Carlo data in the lower P_T region, especially for the normalization scale. We conclude that this is due to the facts that the $c\bar{c}$ cross section in the Monte-Carlo program was not correct (also, P_T^{min} for light quark events was not correct) and that the higher-order effects (order α_s) were not included (for both $c\bar{c}$ and light quark-pair events). The small differences appeared in the slope in the $P_{T,jet}^2$ spectrum. We therefore multiplied the smoothed Monte-Carlo background by a first-order polynomial (a+b $P_{T,jet}^2$). The coefficients (a and b) of the polynomial were set to be free parameters. The signal shapes were assumed to be exponential functions $\propto e^{-P_T/\beta}$. The β at each binning was obtained by fitting Monte-Carlo signal events, and was used as a fixed parameter in the fitting procedures, because the soft-pion angular resolution seemed to be consistent with the prediction of the detector simulation.

The results of the signal and background estimations are shown in Figures 1 (a) - (e) by the solid lines. The peak entries obtained by the above-mentioned procedures are 50 ± 32 , 126 ± 26 , 83 ± 20 , and 113 ± 29 , in the 0.1 - 0.2, 0.2 - 0.3, 0.3 - 0.4, and 0.4 - 0.6 GeV P_T regions, respectively. In total, we obtained 372 ± 54 events.

The main systematic error of the analysis is due to this fitting procedure, since we did not know the exact shapes of the background. We tried various background shapes, such as $(1 + aP_{T,jet}^2 + bP_{T,jet}^4 + cP_{T,jet}^6)^{-1}$ by ALEPH [26] and $(1 + (P_{T,jet}^2/a)^b)^{-1}$ by TOPAZ [21]. We defined the systematic errors of the fitting procedures to be the differences in the obtained peak entries by the various background functions. In addition, we tried to simulate various sets of the Monte-Carlo events by changing the generation parameters described in the previous subsection, and carried out the same fitting procedures. By these procedures, we obtained systematic errors of 12, 23, 18, and 9% in the 0.1 - 0.2, 0.2 - 0.3, 0.3 - 0.4, and 0.4 - 0.6 GeV P_T ranges, respectively.

2.7 Experimental checks of the data sample

We carried out some miscellaneous checks on these peaks. In order to check detector bias, the charge states and the $\cos\theta_{\pi_s}$ distribution were tested. The background-subtracted $P_{T,jet}^2$ distributions are shown in Figures 2 (a) - (d): (a) for π_s^+ , and (b) π_s^- , (c) $\cos\theta_s > 0$, and (d) $\cos\theta_s < 0$. If $D^{*\pm}$'s had originated from single-photon exchange events (for example cascade decays of $b\bar{b}$ events which were produced at low angles with respect to the beam axis), some asymmetries may appear in the charge states, or the $\cos\theta_{\pi_s}$



distribution. These are shown in Figures 2 (e) and (f): (e) charge of π_s multiplied by $\cos\theta_s$ be > 0, and (f) that be < 0. The pairs (a) and (b), (c) and (d), and (e) and (f) seem to be consistent with each other. The numbers of signals in these plots are 190, 182, 202, 169, 168, and 203, respectively, where the statistical errors of them are about 34. In the case of single-photon exchange events ($b\bar{b}$ cascade), the asymmetry of 1:2 should be observed between Figure 2 (e) and (f). In addition, the same checks on the higher P_T events (0.3 $< P_T < 0.6$ GeV) were carried out. The peak entries corresponding to the definitions (a)-(f) were 97, 99, 89, 107, 102, and 94 with the statistical errors of about 20, respectively. They are also consistent with each other. We thus conclude that these events did not originate from single-photon processes.

3 Production cross section

3.1 Systematic ambiguities

This analysis was based on momentum measurements of inclusive pions and jet-axis reconstructions. The former part was well defined and the systematic errors were well known from a previous physics analysis using the TOPAZ detector [28]. The largest systematic error in the tracking algorithm appears especially in the low- P_T region, i.e., the 0.1-0.2 GeV region. The systematic errors were estimated using hadronic events via single-photon exchange processes and the LUND 6.3 Monte-Carlo simulation, since this Monte-Carlo method was known to reproduce many experiments. The thus-obtained systematic errors due to tracking were 7 and 3% at the 0.1 - 0.2 and 0.2 - 0.6 GeV P_T regions, respectively.

The systematic error due to the jet-axis determination were evaluated by changing the maximum value of the invariant mass and the transverse momentum cut in selecting jets by 10%. The errors were 11, 10, 6, and 3% in the 0.1 - 0.2, 0.2 - 0.3, 0.3 - 0.4, and 0.4 - 0.6 GeV P_T ranges, respectively.

The systematic errors in the event selection were estimated in the same way by changing the cut values, such as the visible energy and missing P_T , by 10%, and the sum of charges by one. Those due to the hardware triggers were estimated using a trigger simulation program. For a charged trigger, we added 5% of accidental hits in the tracking detectors. The acceptance was increased by $2\pm 1.4\%$ by this. The percentage of neutral triggered events was only 5.6%. Therefore the systematic errors caused by the energy calibrations of calorimeters and the summing amplifiers noises were considered to be negligible small. In total, the systematic errors were estimated to be 7%.

In total, the systematic errors in determining the production cross sections of the soft-pions were 19, 26, 20, and 12% in the 0.1 - 0.2, 0.2 - 0.3, 0.3 - 0.4, and 0.4 - 0.6 GeV P_T ranges, respectively. From now on, the errors include both the statistical and systematic contributions.

3.2 Soft-pion cross section

We obtained the P_T differential cross section for soft-pions. The P_T of a soft-pion is almost proportional to that of the $D^{*\pm}$, and also to that of the charm quark. In order to define the detector's sensitive area, we restricted the cosine of the soft-pion emission angle with respect to the beam axis to be within ± 0.77 . Then, the acceptance differences, especially between the direct and resolved photon processes, became small ($\pm 5\%$ higher for the resolved photon process). The acceptance was obtained using a Monte-Carlo simulation of the direct and resolved (LAC1) photon processes and it was a increasing function of P_T . The thus-obtained differential cross section is shown in Figure 3 and is listed in Table 1, together with the theoretical predictions (described later).

3.3 $D^{*\pm}$ production cross section

In order to compare this data with the previous results of the $D^{*\pm}$ production at TRISTAN [15], we unfolded the soft-pion cross section to that of $D^{*\pm}$. The method was as follows:

Figure 3: Differential cross section of the soft-pions versus P_T . The histograms are the theoretical predictions: the cross-hatched area is the direct process, the singly-hatched area the resolved process (LAC1), and the open area \tilde{t} pair production.

and the open area \tilde{t} pair production.

P_T range (GeV)	Experiment	Direct	Direct+LAC1	Direct+LAC1+ $\tilde{t}\tilde{t}$
0.1 - 0.2	105 ± 72	81	145	152
0.2 - 0.3	42.3 ± 14.2	18.7	27.1	34.6
0.3 - 0.4	23.4 ± 7.5	6.0	7.5	13.6
0.4 - 0.6	6.4 ± 1.9	1.6	1.9	4.0

Table 1: $d\sigma/dP_T(soft - pion)(|cos\theta| \le 0.77)$ (pb/GeV).

Figure 4: Differential cross section of $D^{*\pm}$ versus P_T . The open circles were obtained from a previous experiment, the open squares are from this experiment, and the closed squares are the combined values. The histogram definitions are the same as those given in Figure 3.

- 1. We tuned the theory by iteratively changing parameters such as the charm-quark mass (current mass) so as to fit the experimental cross section $(d\sigma(D^{*\pm})/dP_T)$ as well as possible. The obtained current charm mass was 1.3 GeV. The details are described in Section 4.
- 2. Using the above parameter, we carried out a simulation and made a conversion matrix from the soft-pion P_T to that of $D^{*\pm}$.
- 3. We multiplied this matrix by the experimental cross section of the soft-pions.

The variation in the P_T spectrum of $D^{*\pm}$ in the Monte-Carlo was a source of systematic error. We therefore assumed various P_T spectra of $D^{*\pm}$ by changing the fragmentation function parameters in LUND 6.3 and tried unfolding. The systematic error of the unfolding was obtained to be 7%. Also there were strong correlations between the neighboring P_T binnings. The largest one was 85% between the binnings 0.1-0.2 and 0.2-0.3 GeV. The magnitudes of the other binning pairs were 30 \sim 40%. The errors due to these correlations were taken into account. The obtained differential cross section of $D^{*\pm}$ is indicated in Figure 4 by the open squares. The previous results are indicated by the open circles [15]. Both experiments are consistent within their errors; the overlapping statistics of the present analysis are obvious. The experimental averages of both measurements are also indicated in Figure 4 by the solid squares and are listed in Table 2, along with the theoretical predictions.

4 Discussion

4.1 Predictions of a two-photon process

4.1.1 Lowest-order calculation

The experimental cross section of $D^{*\pm}$ in the region $1.6 \le P_T \le 6.6$ GeV and $|\cos\theta| \le 0.77$ was 24.2 ± 5.0 pb (Table 2). We first compare this with the lowest-order calculation. A current-charm quark mass of 1.5 GeV and LAC1 parametrization with $\Lambda_{\overline{MS}} = 0.2$ GeV were used. The predictions of the direct and

P_T range	Full	Soft-	Average	Direct	Direct+LAC1	$\text{Direct+LAC1+}\tilde{t}\tilde{t}$
(GeV)	reconstruction	pion				
1.6 - 2.6	22.9 ± 9.7	10.7 ± 5.3	13.5 ± 4.7	7.1	11.8	12.5
2.6 - 3.6	4.80 ± 2.56	5.03 ± 1.88	4.95 ± 1.51	2.42	3.48	4.22
3.6 - 4.6	3.79 ± 1.92	3.01 ± 0.99	3.17 ± 0.88	1.05	1.29	2.08
4.6 - 6.6	1.38 ± 1.23	1.28 ± 0.40	1.29 ± 0.38	0.34	0.41	1.02

Table 2: $d\sigma/dP_T(D^{*\pm})(|\cos\theta| \le 0.77)$ (pb/GeV).

resolved photon processes were 8.5 and 2.5 pb (11.0 pb in total), respectively, significantly lower than the experimental observation.

4.1.2 Higher-order corrections

Corrections on the order of α_s in the QCD part of the theory are available in the analytic calculations [8, 9], but not in the Monte-Carlo calculations. Our Monte-Carlo simulation was based on a lowest-order calculation (LO), which was followed by string fragmentation using LUND 6.3. Since string fragmentation includes a parton-shower-like effect, the next-to-leading-order effect in the P_T spectrum of $D^{*\pm}$ is already counted. For single-photon exchange events, the difference in the momentum spectra of $D^{*\pm}$ between the LO-matrix element (i.e. two-jet only) and the parton-shower options in Lund 6.3 is only 9% at $\sqrt{s} = 10$ GeV. We therefore concluded that the systematic error due to the hadronization process is 9%. We then carried out a next-to-leading-order correction (NLO) (P_T -independently) of the direct process. The factor was 1.31, as described in reference [9]. For the resolved photon process, due to the presence of the process $\gamma q \to c\bar{c}q$ (a part of this is absorbed in the gluon density function in the resolved photon), the P_T dependent factors were obtained in the following way [29]:

- 1. We derived the P_T -dependent ratios between the higher- and lowest-order calculations for both the direct and resolved photon processes.
- 2. We then calculated the ratios between these ratios of the direct and resolved photon processes.
- 3. The final ratios were normalized so as to fit the total cross section of the higher-order calculations for the resolved photon process.

The obtained P_T^c -dependent correction were written as

$$0.50P_T^c + 0.54$$
,

where P_T^c was the P_T of the charm quark in GeV. Here, the charm quark mass (m_c) and the renormalization scale (μ) of 1.6 GeV and $\mu = \sqrt{2}m_c$ were used, respectively. This correction factor was used as event weight in the Monte-Carlo simulations.

Then, the prediction of the cross section in the range $(1.6 \le P_T \le 6.6, |cos\theta| \le 0.77)$ was 15.6 pb, still lower than the experimental observation.

4.1.3 Dependence on the current charm quark mass and gluon P_T distribution

If the current charm-quark mass is significantly lower than 1.5 GeV, the total cross section of $D^{*\pm}$ becomes large. For example, the Monte-Carlo package PYTHIA 5.6 used $m_c = 1.35$ GeV [30]. However, the cross section increased only at a low- P_T region i.e., ≤ 2.6 GeV. The PYTHIA 5.6 program also included a gluon P_T of 0.44 GeV (Gaussian) inside the resolved photon jet. This may increase the high P_T cross section

of $D^{*\pm}$. We thus lowered m_c to 1.3 GeV and added a Gaussian fluctuation in the gluon P_T distribution inside a photon of 0.44 GeV. The obtained cross section was 17.4 pb.

The differential cross sections which this model predicted are given in Figures 3, 4 and Tables 1, 2. The predictions agree with the experimental data in the 1.6 - 3.6 GeV P_T region. However, there is a large excess in the higher P_T regions (> 3.6 GeV).

When we tried other resolved photon parameterization, such as DG [5], the predicted cross sections were significantly lower than the experimental data, even upon changing some of the parameters described so far.

4.1.4 Ambiguities in the prediction

We first estimate the ambiguities in the NLO correction. As has been described, string fragmentation describes a part of the NLO corrections. Therefore, the ambiguities lie in the hard process descriptions, such as three jets and hard bremsstrahlung from the resolved quark line. These are estimated by using the single-photon exchange events generated by the LUND 6.3 Monte-Carlo program. The $D^{*\pm}$ momentum spectra between the LO-matrix with string fragmentation and parton shower options have been compared at \sqrt{s} =10 GeV. A difference of 9% was observed; this was considered to be a systematic ambiguity.

Second, we considered the ambiguities in the charm mass, renormalization scale (μ), and gluon intrinsic P_T inside a photon. The ranges that we selected were $m_c = 1.3 \pm 0.15$ GeV, $m_c < \mu < 2m_c$, and $0 < P_T^{gluon} < 0.44$ GeV, respectively. In total, the cross-section ambiguity was obtained to be 11% for the lower P_T region and 9% for the higher P_T region.

Third, the ambiguity in the equivalent photon approximation was studied. In our event generation, the initial photon from beam was considered to be almost real photon with the direction parallel to the beam axis. We here used a matrix element calculation by Kuroda [31] in the event generation of the direct process. The differential cross section at the higher P_T region was increased by 25% by this effect. We considered that this value is a systematic error due to the Q^2 dependence of $\gamma\gamma$ system in the direct process. In the resolved photon case, we do not know how to take care of this effect. We thus approximated that all photons are real photons. We considered this systematic error due to the motion of $\gamma\gamma$ system is absorbed in that of the intrinsic gluon P_T inside the photon.

Last, the threshold effect of the $c\bar{c}$ productions are commented. The Wvis distribution, i.e., the invariant mass of visible hadronic system, are shown in Figure 6 (a) and (b) for the lower and higher P_T soft-pion signals. They were dominated in the region where Wvis > 5 GeV. The real $W_{\gamma\gamma}$ was expected to be distributed above this value. We therefore concluded that the threshold effect was small in our detection region. We did not consider about the systematic ambiguity due to the threshold enhancement by this reason.

The experimental excess at the high- P_T region $(P_T(D^{*\pm}) > 3.6 \text{ GeV})$ with respect to the theoretical prediction of the direct plus resolved (LAC1) photon processes becomes a 2.9σ effect.

4.2 Possibility of \tilde{t} pair production

One of the exciting possibilities to explain this excess is in terms of \tilde{t} pair production. A light \tilde{t} at the TRISTAN energy region is still possible if the mass difference between \tilde{t} and $\tilde{\gamma}$ is small [16, 17, 18, 19]. In a previous paper [20], in order to explain the high P_T excess of $D^{*\pm}$, \tilde{t} pair production was introduced with $m_{\tilde{t}}=15$ GeV and $m_{\tilde{\gamma}}=12.7$ GeV. These predictions are shown in Figures 3 and 4 by open histograms. The experimental cross sections agree very well with these assumptions. The value of $m_{\tilde{t}}$ determines the cross-section excess and that of $m_{\tilde{\gamma}}$ the event shapes, such as the thrust and missing P_T distributions. These two distributions are shown in Figures 5 (a)-(d). Here, we had problems in translating the number of events into cross sections. We thus plotted the observed number of events with the theoretical predictions. In addition, our Monte-Carlo generator did not include any higher order (α_s) effect, such as three-jet

Figure 5: Various event shape distributions for the lower $(P_T < 0.3 \text{ GeV})$ and higher $(P_T > 0.3 \text{ GeV})$ P_T events: (a) thrust distribution in the lower P_T events, (b) that in the higher P_T region, (c) missing P_T distribution in the lower P_T region, (d) that in the higher P_T region, (e) $|\cos\theta|$ distribution of the soft-pions in the lower P_T region, and (f) that in the higher P_T region. The histogram definitions are the same as those given in Figure 3.

events. One should therefore be cautious about them. The real thrust predictions may be softer and that of the missing P_T distributions may be harder due to the presence of three-jet events.

From these figures, the experimental excesses are considered to be high-thrust events and high missing- P_T events. In order to minimize this discrepancy in the missing P_T -distribution, although we must set a larger mass difference $(m_{\tilde{t}} - m_{\tilde{\gamma}})$, it may conflict with the recent search for \tilde{t} pair production by the VENUS experiment [32].

If the excess is due to \tilde{t} pair production, the angular distribution with respect to the beam axis must be different from that of the two-photon processes. The results are also shown in Figures 5 (e) and (f). However, the \tilde{t} assumption does not show good agreement. The excess events dominated in the low-angle region. We therefore can not strongly conclude that the excess in events originated from \tilde{t} pair production. There is a possibility of a new high- P_T process in the two-photon interaction. If this is true, it would be a serious background in future linear-collider experiments.

In addition, we checked three more distributions, i.e., Wvis, the rapidity of the hadronic system, and the azimuthal angle between the missing P_T and the soft-pions as shown in Figures 6 (a)-(f). These distributions does not fit to the \tilde{t} assumption very well. We definitely need more studies on this process. Especially the electron and/or K-meson inclusive studies would be more powerful because of higher statistics.

4.3 Tagged events

In a part of the data set (integrated luminosity of 90 pb⁻¹), there were forward calorimeters (FCL; made of BGO) which covered the polar angle region at between 3.2 and 13.6 degrees [33]. We analyzed tagged events using the FCL with the same analysis. We observed 35.5 ± 12.7 soft-pions, where the lowest-order direct process predicts ~ 26.7 events. The tagged events are therefore consistent with the expectation.

4.4 Comparison with other experimental results

The charm measurement using the inclusive electron method was pioneered by the VENUS group [34]. Their observed production rate was consistent with a theoretical prediction by the direct and resolved (LAC1) processes. However, the statistics are especially low in the high- P_T^c region. The expected \tilde{t} signal rate was only a few events. We thus concluded that the VENUS measurement was not sensitive to the \tilde{t} signal, and was consistent with our observation. A high-statistics study using high P_T electrons is awaited.

Recently, a \tilde{t} search was carried out by the VENUS group [32]. They have shown an $m_{\tilde{\gamma}}$ upper limit of ~ 12.7 GeV for the case when $m_{\tilde{t}} = 15$ GeV. This search marginally conflicts with our \tilde{t} assumption.

5 Conclusions

We have measured the differential cross section $(d\sigma(e^+e^- \to e^+e^-D^{*\pm}X)/dP_T)$. The $D^{*\pm}s$ were identified by the transverse momenta of soft-pions with respect to the jet-axes. The average \sqrt{s} was 58.1 GeV and the integrated luminosity of the event sample was 198 pb⁻¹, respectively. We obtained 372 \pm 54 $D^{*\pm}$, which represents the highest statistics so far obtained. We compared the measured cross section with the theoretical predictions.

Acknowledgement

We appreciate discussions with Prof. M. Kobayashi (KEK), Dr. M. Drees (Univ. of Wisconsin), M. Krämer (DESY), and J. Zunft (DESY). We thank the TRISTAN accelerator staff for the successful operation of TRISTAN. We also thank all of the engineers and technicians at KEK as well as members

Figure 6: Various event shape distributions for the lower $(P_T < 0.3 \text{ GeV})$ and higher $(P_T > 0.3 \text{ GeV})$ P_T events: (a) Wvis distribution in the lower P_T events, (b) that in the higher P_T region, (c) rapidity of hadronic system in the lower P_T region, (d) that in the higher P_T region, (e) cosine of the azimuthal angle between the missing P_T and the soft-pion in the lower P_T region, and (f) that in the higher P_T region. The histogram definitions are the same as those given in Figure 3.

of the collaborating institutions: H. Inoue, N. Kimura, K. Shiino, M. Tanaka, K. Tsukada, N. Ujiie, and H. Yamaoka.

References

- [1] See e.g. S. J. Brodsky, T. Kinoshita, and H. Terazawa, Phys. Rev. D4 (1971) 1532.
- [2] S. J. Brodsky, T. A. DeGrand, J. F. Gunion, and J. H. Weis, Phys. Rev. Lett. 41 (1978) 672; Phys. Rev. D19 (1979) 1418.
- [3] H. Terazawa, J. Phys. Soc. Japan, 47 (1979) 355.
- [4] K. Kajantie and R. Raitio, Nucl. Phys. **B159** (1979) 528.
- [5] M. Drees and K. Grassie [DG], Z. Phys. C28 (1985) 451.
- [6] H. Abramowicz, K. Charchula, and A. Levy [LAC], Phys. Lett. **B269** (1991) 458.
- [7] M. Glück, E. Reya, and A. Vogt [GRV], Phys. Rev. **D46** (1992) 1973.
- [8] J. Smith and W. van Neerven, Nucl. Phys. **B274** (1992) 36.
- [9] M. Drees, M. Krämer, J. Zunft, and P. M. Zerwas, Phys. Lett. **B306** (1993) 371.
- [10] R. Tanaka et al., Phys. Lett. **B277** (1992) 215.
- [11] H. Hayashii et al., Phys. Lett. **B314** (1993) 149.
- [12] W. Bartel et al., Phys. Lett. **B184** (1987) 288.
- [13] W. Braunschweig et al., Z. Phys. C47 (1990) 499.
- [14] M. Alston-Garnjost et al., Phys. Lett. **B252** (1990) 499.
- [15] R. Enomoto et al., Phys. Rev. **D** 50, 1879 (1994).
- [16] K. Hikasa and M. Kobayashi, Phys. Rev. **D36** (1987) 724.
- [17] I. Adachi et. al., Phys. Lett. **B218** (1989) 105.
- [18] Y. Sakai et al., Phys. Lett. **B234** (1990) 534.
- [19] M. Drees and K. Hikasa, Phys. Lett. **B252** (1990) 127.
- [20] R. Enomoto et al., KEK-preprint 93-107 (1993), unpublished.
- [21] E. Nakano et al., Phys. Lett. **B314** (1993) 471.
- [22] R. Enomoto et. al., Nucl. Instrum. Methods, A269 (1988) 507; A. Imanishi et. al., Nucl. Instrum. Methods, A269 (1988) 513; T. Kamae et. al., Nucl. Instrum. Methods, A252 (1986) 423; A. Yamamoto et. al., Jpn. J. Appl. Phys. Lett., 25 (1986) L440; S. Kawabata et. al., Nucl. Instrum. Methods, A270 (1988) 11; J. Fujimoto et. al., Nucl. Instrum. Methods, A256 (1987) 449; S. Noguchi et. al., Nucl. Instrum. Methods, A271 (1988) 464.
- [23] "Review of Particle Properties", Phys. Rev. **D45** (1992), Part II.

- [24] T. Sjöstrand, Comput. Phys. Commun., **39** (1986) 347; T. Sjöstrand and M. Bengtsson, Comput. Phys. Commun., **43** (1987) 367. The symmetric LUND fragmentation function with $\sigma_q = 0.42$, a=0.9, and b=0.61 without parton shower option was used. These parameters were fitted with single γ annihilation hadronic events, which was described in I. Adachi et al., Phys. Lett. **B227** (1989) 495. These parametrization also reproduce charm meson fragmentation function at lower energies.
- [25] F. Butler et al., Phys. Rev. Lett. 69 (1992) 2041.
- [26] D. Decamp et al., Phys. Lett. **B266** (1991) 218.
- [27] D. Bortoletto et al., Phys. Rev. **D37** (1988) 1719; **D39** (1989) 1471.
- [28] I. Adachi et al., Phys. Lett. **B227** (1989) 495.
- [29] Private communication with M. Drees, M. Kämer, and J. Zunft.
- [30] T. Sjöstrand, CERN-TH 6488/92.
- [31] M. Kuroda, Meiji Gakuin University (Tokyo), Res. J. 424 (1988) 27; Meiji Gakuin University preprint, MGU-DP 7 (1988), unpublished.
- [32] J. Shirai et al., Phys. Rev. Lett., 23 (1994) 3313.
- [33] H. Hayashii et al., Nucl. Instrum. Method., A316 (1992) 202.
- [34] S. Uehara et al., Z. Phys. C 63 (1994) 213.

This figure "fig1-1.png" is available in "png" format from:

This figure "fig1-2.png" is available in "png" format from:

This figure "fig1-3.png" is available in "png" format from:

This figure "fig1-4.png" is available in "png" format from:

This figure "fig1-5.png" is available in "png" format from:

This figure "fig1-6.png" is available in "png" format from:

